Endothelial repair process and its relevance to longitudinal neointimal tissue patterns: Comparing histology with in silico modelling

Tahir, H.; Bona-Casas, C.; Narracott, A.J.; Iqbal, J.; Gunn, J.; Lawford, P.; Hoekstra, A.G.

DOI
10.1098/rsif.2014.0022

Publication date
2014

Document Version
Final published version

Published in
Journal of the Royal Society Interface

JOURNAL OF THE ROYAL SOCIETY Interface

rsif.royalsocietypublishing.org

Research

Cite this article: Tahir H, Bona-Casas C, Narracott AJ, Iqbal J, Gunn J, Lawford P, Hoekstra AG. 2014 Endothelial repair process and its relevance to longitudinal neointimal tissue patterns: comparing histology with *in silico* modelling. *J. R. Soc. Interface* **11**: 20140022.
http://dx.doi.org/10.1098/rsif.2014.0022

Received: 9 January 2014
Accepted: 19 February 2014

Subject Areas:
biomedical engineering

Keywords:
computer modelling, in-stent restenosis, re-endothelialization, neointimal patterns, endothelial cells

Author for correspondence:
Hannan Tahir
e-mail: h.tahir@uva.nl

Royal Society Publishing

Endothelial repair process and its relevance to longitudinal neointimal tissue patterns: comparing histology with *in silico* modelling

Hannan Tahir[1], Carles Bona-Casas[1], Andrew James Narracott[2], Javaid Iqbal[3], Julian Gunn[3], Patricia Lawford[2] and Alfons G. Hoekstra[1,4]

[1]Computational Science, Informatics Institute, University of Amsterdam, Science Park 904, Amsterdam 1098 XH, The Netherlands
[2]Medical Physics Group, Department of Cardiovascular Science, and [3]Coronary Artery Disease Group, Department of Cardiovascular Science, University of Sheffield, Sheffield, UK
[4]National Research University ITMO, Saint Petersburg, Russia

Re-establishing a functional endothelium following endovascular treatment is an important factor in arresting neointimal proliferation. In this study, both histology (*in vivo*) and computational simulations (*in silico*) are used to evaluate neointimal growth patterns within coronary arteries along the axial direction of the stent. Comparison of the growth configurations *in vivo* and *in silico* was undertaken to identify candidate mechanisms for endothelial repair. Stent, lumen and neointimal areas were measured from histological sections obtained from eight right coronary stented porcine arteries. Two re-endothelialization scenarios (endothelial cell (EC) random seeding and EC growth from proximal and distal ends) were implemented *in silico* to evaluate their influence on the morphology of the simulated lesions. Subject to the assumptions made in the current simulations, comparison between *in vivo* and *in silico* results suggests that endothelial growth does not occur from the proximal and distal ends alone, but is more consistent with the assumption of a random seeding process. This may occur either from the patches of endothelium which survive following stent implantation or from attachment of circulating endothelial progenitor cells.

1. Introduction

In-stent restenosis (ISR), the re-narrowing of the stented artery after percutaneous coronary intervention (PCI), represents an exaggerated healing response to iatrogenic injury to the vessel wall during angioplasty and stenting [1,2]. In comparison with bare metal stents (BMS), drug-eluting stents (DES) have dramatically reduced the rates of ISR [3]. However, the antiproliferative drugs eluted from DES not only impair smooth muscle cell (SMC) growth underlying ISR, but also delay endothelial regrowth which increases the risk of stent thrombosis [4,5]. Prolonged dual anti-platelet treatment is required to prevent this potentially fatal complication of PCI.

Understanding the process and mechanism of endothelial regeneration after PCI is clinically important but remains poorly understood to date. In the 1970s, a number of studies reported the role of endothelial cell (EC) migration and proliferation from nearby un-injured ECs in the regeneration of endothelium at the site of injury [5,6]. However, other studies provided evidence to support the development of mature ECs from the homing of endothelial progenitor cells (EPCs) within the blood [7,8]. In the past decades, intensive effort has been undertaken to understand the biological properties of EPCs and their relevant contribution towards endothelial repair, but the results are still conflicting [9,10]. Some recent reports suggest that EPC may not contribute directly to regrowth of the endothelium during the vascular healing process [9] and perhaps, the only valid

mechanism involved is proliferation and migration of the ECs from the edges of the injured area [9,11].

Porcine experiments have been helpful to understand the dynamics of the complex restenotic process and the underlying mechanisms. Combining such data with the outcomes from numerical simulations can inform understanding of such processes and allows the testing of new hypotheses. Both the degree of restenosis and the distribution of neointima along the length of the stent may be influenced by not only the endothelial growth rate [12] but also the origin of endothelial regeneration. In this study, we report the variation of neointimal growth along the length of a stented artery *in vivo* through analysis of the variability in growth patterns from porcine coronary histological sections. The response of the stented artery is simulated to provide *in silico* data from a two-dimensional computational model where two different re-endothelialization scenarios were incorporated which focus on the effect of the origin of endothelial regeneration (random EC seeding and EC growth from proximal and distal ends). Results from these two different scenarios were then compared with the averaged trends of the *in vivo* data to identify the most probable mechanism of re-endothelialization during vascular healing.

2. Material and methods

2.1. Animal experiments

For the purpose of this study, the arteries treated with BiodivYsio BMS (3.5 × 15 mm) are taken into account. All animal work was carried out under UK Home Office license in accordance with the Animals (Scientific Procedures) Act, 1986 and conforms to the Guide for the Care and Use of Laboratory Animals published by the US National Institutes of Health.

All angiographic procedures were performed under general anaesthesia; induced with intravenous propofol at a dose of 4 mg kg^{-1} and maintained with inhaled isoflurane 5% in oxygen via an endotracheal tube. The experimental protocol has been described in detail elsewhere [13,14]. In total, data from eight coronary arteries were used where stents were deployed in the right coronary arteries (RCAs). Balloon pressure was kept at 8 atmospheric pressure for 30 s to allow the deployment of the stents. Heparin (2500 U) was injected before the interventional procedure, and 150 mg of aspirin was administered orally for 5 days. Animals were sacrificed at 28 days post-stenting, and stented arteries were harvested from the animal. Histological sections from the stented vessels were processed using a previously published technique [15] where the dissected stented arteries were first perfusion fixed in 10% formalin and then embedded into a T8100 resin. Once embedded, arterial segments were cut into approximately 18–22 sections using a diamond-tipped saw and were then ground and polished to a section thickness appropriate for light microscopy [13,14]. Each section was investigated under a microscope, and images of the histological section were saved digitally for post-processing (figure 1*a*,*b*). The resolution of the microscope was kept constant for all sections, and the scale at which images were saved was 3.22 μm per pixel.

2.2. *In vivo* post-processing method

The digital histology images were post-processed using Matlab (MathWorks, Inc.) to calculate stent, lumen and neointimal areas. The stent boundary was identified by manually selecting points at the centre of each stent strut, the lumen boundary was identified by manual identification of the lumen boundary. Both methods assume the area is bounded between points by a straight line. A centre point was identified, and triangles were constructed for both stent (figure 1*c*) and lumen (figure 1*d*) by selecting two surface points and the centre point. The area of each triangle was calculated through the vector cross product method using the equation shown

$$\text{area} = \frac{1}{2}\,|\boldsymbol{v}_i \times \boldsymbol{v}_{i+1}|\,,$$

where $\boldsymbol{v}_i$ and $\boldsymbol{v}_{i+1}$ are the vectors pointing from the centre point P_c to point P_i and P_{i+1}, respectively (figure 1*c*).

$$\text{Total area for a given section (stent or lumen)} = \sum_{i=1}^{N} \text{area}_i,$$

where N denotes the number of triangles made from points in a given section. Neointimal area was obtained by subtracting lumen area from the stent area. As the measurement was a manual procedure, it was repeated five times, for each section of every artery, to assess the errors involved in manual selection (figure 1*e*).

2.3. *In silico* model

A computational two-dimensional multi-scale model of ISR has already been developed [16–18] and has been recently used to study the effect of re-endothelialization rate and subsequent release of nitric oxide (NO) on the regulation of SMCs [12].

Haemodynamics plays a crucial role during the generation of ISR, therefore such a complex process can perhaps be better modelled by decomposing the overall process into single scale models. Currently, we consider two single scale models: (i) blood flow, and (ii) tissue growth. These single scale models are coupled to each other using the multi-scale coupling library and environment (MUSCLE) [19–22].

2.3.1. Vascular geometry

In this study, the vessel length has been increased by a factor of three compared with our previous model domains. Simulation of a longer vessel allows more stent struts to be deployed compared with our previous benchmark geometries, allowing investigation of the morphological changes in neointima along the length of the stent under different endothelial regrowth scenarios. We considered a vessel of a length of 4.5 mm with a lumen width of 1 mm. The model was initialized by generating the vessel wall composed of five layers of densely packed SMCs on each side. The diameter of each SMC was defined as 30 μm; based on the selected packing density this produced a vessel wall thickness of 120 μm, equivalent to the average medial thickness observed in histological sections [23]. A thin layer of internal elastic lamina (IEL) was also generated at the vessel lumen (on top of SMCs) on both sides of the vessel (upper and lower). Six BMS struts were deployed to a depth of 110 μm into the tissue, three on each side of the vessel wall. During the deployment procedure, IEL cells were removed based on the longitudinal, and hoop stresses with rupture of the IEL providing an estimate of the injury in the tissue owing to stent deployment. We assume complete removal of the endothelium owing to the balloon angioplasty, whereas the stent struts rupture the IEL layer. The stented vascular geometry is then passed to the coupled blood flow and tissue growth models.

2.3.2. Blood flow model

Steady-state blood flow inside the stented vessel at Reynolds number ($Re = 120$) was modelled using a standard BGK lattice Boltzmann method (LBM), assuming blood to be a Newtonian incompressible fluid with a constant viscosity, $\mu = 4$ mPa s, density $\rho = 1000$ kg m^{-3}. Based on the magnitude of the Reynolds number, $Re = 120$, which is within the physiological

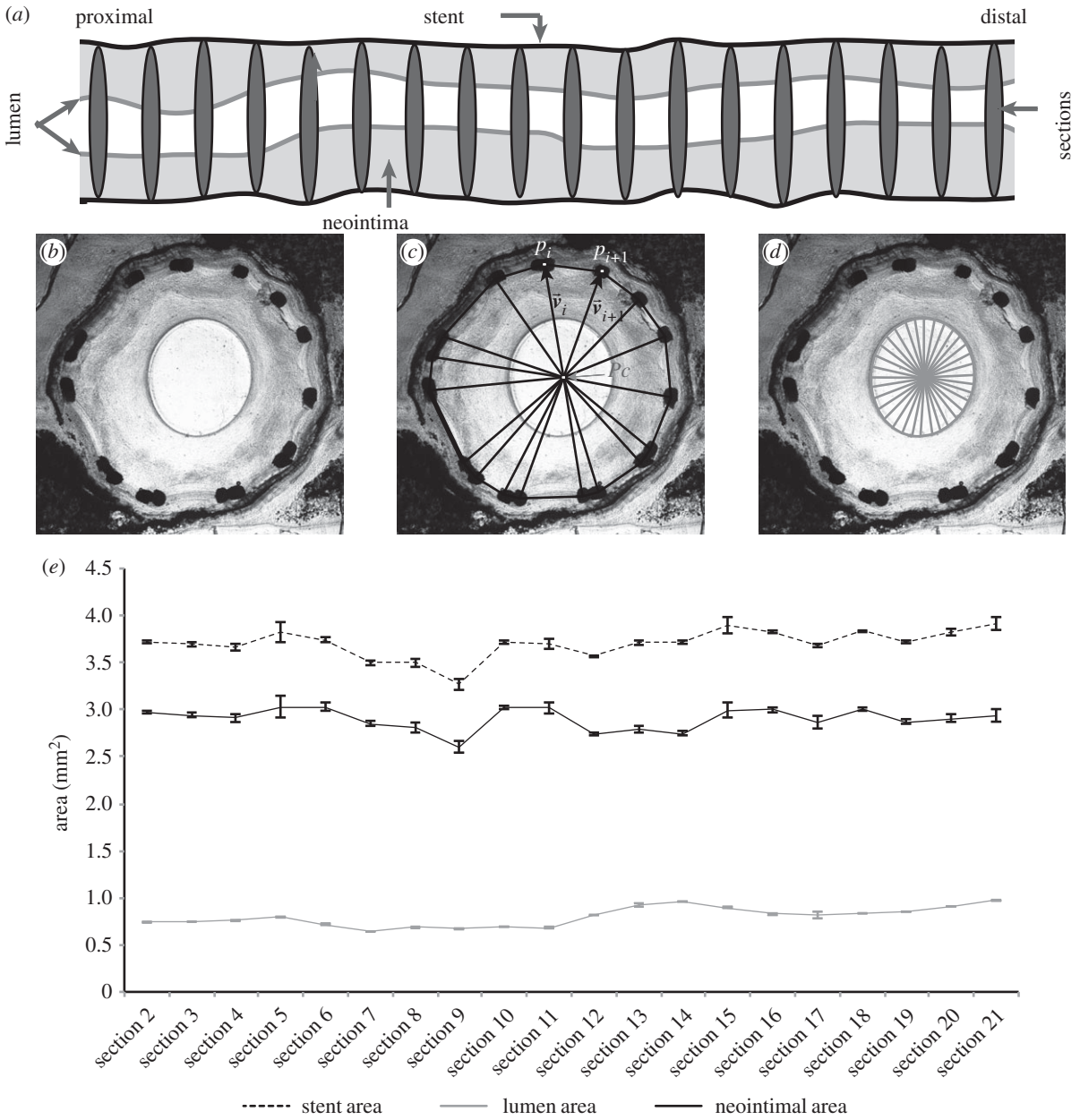

Figure 1. Histological sections and post-processing area calculations. (*a*) Idealized representation of the vessel where each circle represents one of the histology sections. (*b*) A representative histology section. Post-processing techniques to calculate (*c*) stent area and (*d*) lumen area. (*e*) Example of one artery showing an average result of the standard human error involved during the post-processing method for the stent, lumen and neointimal areas calculations. The error bars represent the standard deviation in the results.

range, the notion of laminar flow is completely justified. To perform LBM simulations, every iteration of the coupled model includes conversion from cell-based stented geometry into a grid-based computational mesh. Periodic boundary conditions were enforced at the inlet and outlet, whereas a velocity Dirichlet boundary condition using the bounce-back rule was imposed at the inner vessel wall. The choice of using periodic boundaries in this study was merely due to technical reasons. However, we ran some initial test trials where we looked at the effects of the periodic boundary conditions (data not shown). Testing of the influence of the boundary conditions was undertaken during the initial stage of the model development by extending the length of the vessel and then comparing the results with those for a shorter vessel. The resultant shear stresses and neointimal growths were comparable, and there were no significant differences observed. The wall shear stress (WSS) on the inner vessel wall was computed from the flow simulations, and this parameter was then mapped back from the lattice grid onto individual cells in the tissue growth model.

2.3.3. Tissue growth model

The dynamics of the vascular tissue composed of SMCs is simulated using an agent-based model (ABM) where each cell is independently modelled as an agent. Every iteration of the tissue model contains two solvers:

(i) *Physical solver*: this solver is responsible for computing the equilibrium positions of the SMCs based on the intercellular forces (attractive, repulsive). The repulsive force between cells is computed as a function of the separation between the centres of two cylindrical bodies with parallel axes, based on Hertzian contact [24,25].

Assuming Hertzian contact, the contact force per unit length is

$$F_{\mathrm{H}} = \frac{a^2}{4} \cdot E^* \cdot \pi \cdot \left(\frac{1}{R_1} + \frac{1}{R_2} \right),$$

where R_1 and R_2 are the radius of both cylinders, $E^* = (E/1 - v^2)$ with E the elastic Young modulus and v the Poisson ratio.

Additionally, we may define a as the radius of the contact area

$$a = \frac{\sqrt{R_1^2 \cdot R_2^2 - 0.25 \cdot (s^2 - (R_1^2 + R_2^2))^2}}{s},$$

where s is the distance between the centres of both cylinders. If it is assumed that there is an attractive force per unit length that is proportional to the contact length, with a constant of proportionality K:

$$F_A = 2aK.$$

Then, the total force per unit length between two cylindrical bodies is

$$F = 2aK - \frac{a^2}{4} \cdot E^* \cdot \pi \cdot \left(\frac{1}{R_1} + \frac{1}{R_2}\right).$$

Every iteration of the physical solver involves computing the new equilibrium positions of the SMCs using Newton's second law of motion. Neglecting inertial terms, the model is described by the equation

$$C\frac{\mathrm{d}x}{\mathrm{d}t} = F(t, x, r),$$

where x is the vector of cell displacements, r is the vector of cell radii and C is a matrix of friction coefficients. A measure of stress is also computed by adding the absolute magnitudes of all the forces applied to the cell in each of the radial and axial directions.

The rationale for choosing the ABM to represent the bulk behaviour of the vascular tissue is mainly due to its intuitive power to incorporate cell growth via the cell cycle. The bulk behaviour of the tissue is assessed based on the chosen cell–cell force interaction law and currently, we do not explicitly incorporate the behaviour of extracellular matrix (the major structural component of tissues). Furthermore, it has also been observed that the qualitative large-scale behaviour of the cell ensemble does not change on varying the exact form of the interaction cell–cell force law [26].

(ii) *Biological solver*: this solver simulates the cell cycle based on the biological rule set. The growth and division of the SMC is described as distinctive phases of the cell cycle: quiescent state G0, a growth state G1 and a mitotic stage S/G2/M where a parent cell divides into two daughter cells. The cell cycle evolution takes place at a prescribed rate based on porcine SMC cell cycle data [27] and finally reaches a peak when mitosis occurs. The average cell cycle duration of the porcine SMCs from the point of entering the G1 phase to division into two daughter cells is 32 h [27]. A cell can enter or leave the G0 (inactive phase) depending on certain rules, which include contact inhibition (based on the neighbour count) and the presence of NO. NO is produced by a functional endothelium in response to fluid shear stresses, higher concentrations of NO are assumed to arrest the cell cycle during the G1 phase and return the cell to a quiescent state. Further details related to the formulation of the cell cycle have been explained in our previous publication [12].

2.3.4. Endothelium regeneration and smooth muscle cell regulation

Based on published material [28], a complete denudation of the endothelium was assumed immediately after balloon angioplasty and stenting. It has also been identified that endothelium regenerates as part of the vascular healing process [29]. Once endothelium is present, it is assumed to respond to the shear stresses generated by the blood flow and produce NO based on shear stress magnitude. The concentration of NO is then used to inform the process of cell cycle arrest in the adjacent SMCs, as described above. If there is no endothelium present adjacent to an SMC, then it will continue to proliferate, giving rise to neointimal development. In the current model, no distinction is made between functional and non-functional endothelium, once endothelium has been generated it is assumed to immediately respond to shear stress stimuli. Therefore, we assume that any endothelium which is not yet mature/functional does not play a significant role. The generation of NO from shear stress has been estimated by extrapolating the data provided by Guo *et al*. [30], these details are reported in our previous paper [12]. Nakazawa *et al*. [31] observed the time course of endothelial regeneration in stented porcine coronary arteries and assessed its functionality by means of platelet endothelial cell adhesion molecule (PECAM-1). A 94% PECAM-1 expression in the stented arteries was observed after 14 days post-stenting [31]. We have extrapolated and used the time course information provided by Nakazawa *et al*. to study other delayed re-endothelialization situations in our previous paper [12]. In this study, we assume that 100% endothelial recovery occurs 23 days post-stenting, as previously described [12]. ECs are not modelled explicitly in this study. A probability function indicating the presence of a healthy endothelium is used starting with 0% endothelial coverage immediately after stenting and incrementally seeding ECs within the domain at a fixed recovery rate. This fixed recovery rate (4.35% per day) has been determined by computing the slope of a straight line between 0% (at day 0) and 100% (at day 23rd) endothelial coverage.

2.3.5. Re-endothelialization scenarios

In silico results were produced under two distinct re-endothelialization scenarios. These scenarios represent possible behaviour of EC function following stenting as reported in the literature. The first scenario involves the regeneration of EC from either side of the stented region (the proximal and distal boundaries of the model) assuming complete endothelial denudation owing to balloon angioplasty and stent deployment. This scenario of EC proliferation from both sides inward was highlighted by Itoh *et al*. [11], where the endothelium was completely denuded within the injured area. However, this complete removal of the endothelial layer was largely dependent on the experimental set-up and the nature of endothelial damage. The second scenario, described previously [12], involves random seeding of ECs, assumed to be a result of either endothelial patches remaining after the balloon angioplasty/stenting procedure and/or from homing of circulating EPCs to the site of injury. Harnek *et al*. [28] have suggested that there may be patches of surviving endothelium in stented segments, but the exact location of these leftover patches is not known and the percentage of remaining endothelium appears to be stent design-dependent [28].

For both scenarios, it is assumed that 100% endothelium recovery occurs at 23 days post-stenting, as previously described [12]. The obvious difference in the above scenarios is the evolution of the spatial distribution of endothelium on the inner layer of the vessel as a function of simulation time.

To compare with the processing applied to the *in vivo* data, the surface area of the stent, lumen and neointima are computed *in silico*. For the area estimation, rectangles were made with a height corresponding to the distance between the inner boundaries for both stent and lumen, whereas the width of the rectangles is chosen to be equivalent to the diameter of one SMC (30 μm). For the height of the stent rectangle, centre points in the middle of struts are chosen (figure 2) similar to the measurements carried out in the *in vivo* data, however, for the lumen, the inner most cells in the upper and lower half were identified within the width of the rectangular window and the distance between those two points was calculated (figure 2). The area of the rectangles is computed by multiplying the width by the height. These rectangles, both stent and lumen with a width equivalent to one SMC diameter, were moved from the proximal to the distal end using a step size of 30 μm in order to compute the area along the axial direction.

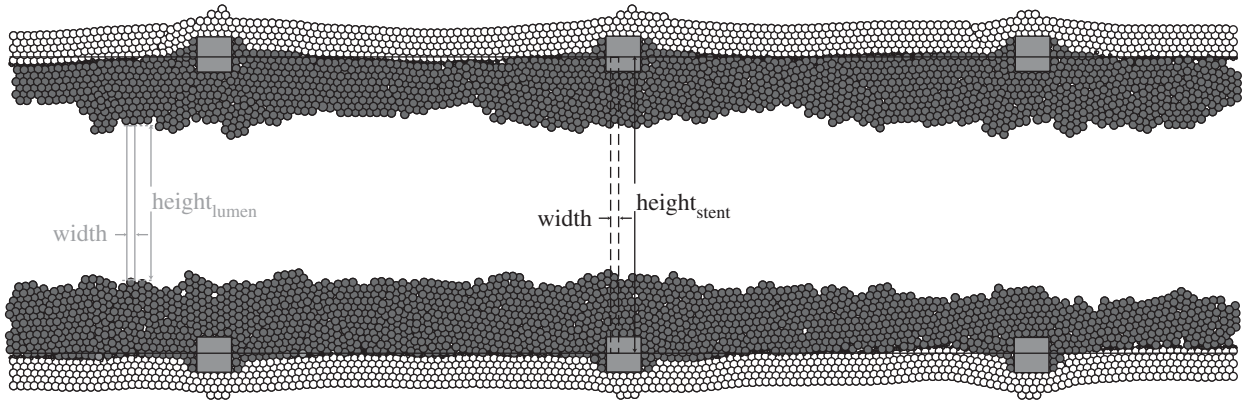

Figure 2. Surface area measurement procedure to calculate stent and lumen areas by making rectangles using stent and lumen boundaries. Neointimal area is obtained by subtracting lumen area from the stent area. The six grey squares represent stent struts deployed in the vessel. The tissue composed of white SMC cells underneath the struts shows the original vessel after stent deployment. However, dark grey SMCs represent the neointima in both scenarios.

2.4. Statistical analysis

For both *in vivo* and *in silico* results, the descriptive statistics (stent, lumen and neointimal areas) are expressed as mean $\pm$ s.d. Comparison of both *in silico* scenarios with the *in vivo* data used un-paired *t*-tests where a difference of $p < 0.05$ was regarded as statistically significant.

3. Results

3.1. *In vivo* results

The stent, lumen and neointimal areas were measured five times for each section of all arteries to obtain a measure of the error associated with post-processing, this error is shown for one artery in figure 1*e*. The most proximal and distal sections were excluded from analysis as these sections were obtained very close to the end of the stent geometry, and in some cases, an incomplete ring of struts excludes the possibility of computing the stent area. The number of sections in each artery were normalized to a fractional length of 1 along the stent as the *x*-axis in the plot shown in figure 3*a*, with 0 corresponding to the first section analysed at the proximal end and 1 corresponding to the last section analysed on the distal side. The percentage stenosis owing to neointima in each section was obtained using the mean value of stent area of each section from the five repeated measurements. The variation in percentage stenosis along the stent is shown for all eight RCAs in figure 3*a*. Comparison of the growth at the proximal and distal edges of all arteries indicates that six arteries showed higher neointimal growth at the distal end, with only two arteries showing equal or slightly lower neointima at the distal end. However, the difference in percentage stenosis between each end is not statistically significant ($p = 0.16$). To better understand the growth trends, linear regression was applied to the neointimal area data for each artery to characterize the variation in slope from the proximal to distal ends. Analysis of the regression showed that almost all arteries have a small but positive slope except one where the slope was -0.00118 ± 0.0047 (neointimal area per normalized length, whereas $\pm$ represents the standard slope error).

3.2. *In silico* results

Morphological differences in the simulated tissue growth patterns were observed between the two EC regeneration scenarios. The *in silico* results demonstrate a strong effect of

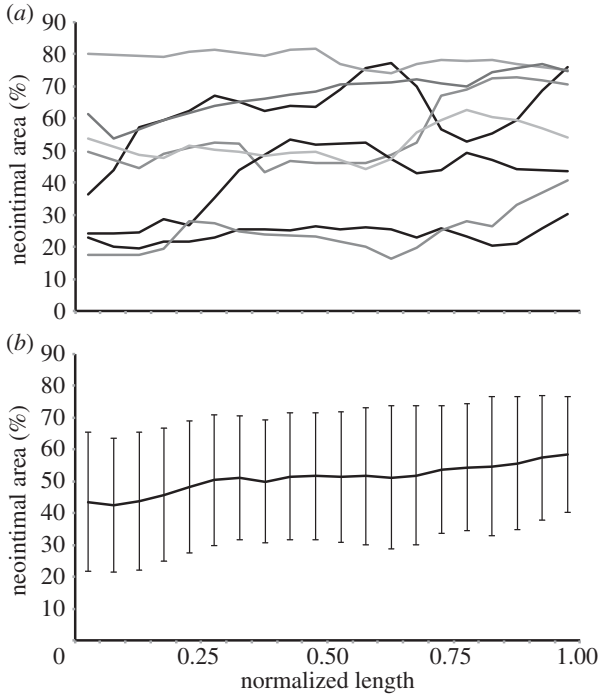

Figure 3. *In vivo* variation in the percentage stenosis due to neointimal growth along the length of the stented segment, measured from histology. (*a*) Percentage of neointimal area in all eight RCAs. (*b*) An averaged result of neointimal area percentage from all the arteries (shown in figure 3*a*) while the vertical error bars show the standard deviation.

the two extreme scenarios of EC regrowth. Random seeding of ECs resulted in a relatively homogeneous distribution of neointima along the stented length (figure 4*a*), whereas the specification of endothelial growth from both sides results in a thicker neointimal lesion in the middle of the stented vessel (figure 4*b*). These morphological differences are clearly evident with the use of the same re-endothelialization growth rate. Stent, lumen and neointimal area computed *in silico* are shown in figure 5*a*,*b* where neointimal area is obtained by subtracting the lumen area from the stent area. The neointimal area trends (from the proximal to the distal end) are significantly different, especially in the centre of the stented area and at the extremes (proximal and distal ends). As for the *in vivo* results, the percentage stenosis was calculated and is shown in figure 5*c* along with the standard deviation of results obtained from six simulation runs. Figure 5*c*

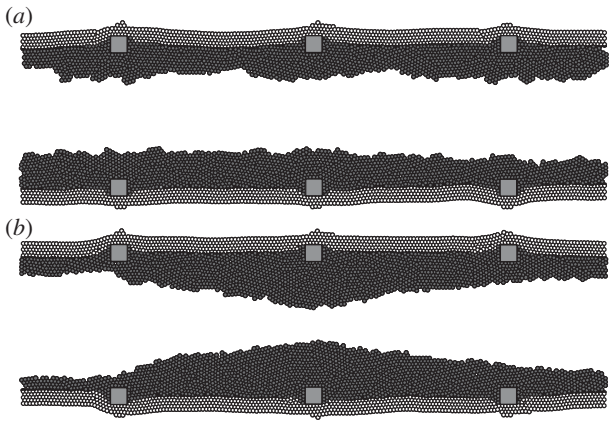

Figure 4. Computational results showing qualitative morphological differences in neointimal growth between the two re-endothelialization scenarios: (*a*) random seeding of ECs and (*b*) inward EC growth from both sides. The six grey squares in each figure represent stent struts deployed in the vessel. The tissue composed of white SMC cells underneath the struts shows the original vessel after stent deployment. However, dark grey SMCs represent the neointima in both scenarios.

shows a distinct peak in the middle of the stented vessel when EC regeneration is assumed to occur from both sides, with the random seeding scenario resulting in a more homogeneous (less pronounced peaks) neointimal growth within the vessel.

3.3. Histological and simulation results comparison

To compare the two *in silico* endothelial regeneration scenarios with the *in vivo* results to examine how well each scenario agrees with the growth trends observed from histology, the ratio of neointimal area at each location relative to that at the centre of the stented section was calculated. These ratios are defined as

$$\text{ratio}_{\text{proximal to centre}} = \frac{\text{neointimal area } N}{\text{neointimal area at proximal end}},$$

and

$$\text{ratio}_{\text{distal to centre}} = \frac{\text{neointimal area } N}{\text{neointimal area at distal end}},$$

where neointimal area N is the neointimal area at each histological section. Figure 6*a*,*b* shows the averaged outcome of proximal to centre and distal to centre ratio calculations respectively for all the arteries along with the modelling results of both endothelium scenarios. So, a uniform growth will give a straight line at 1 and any deviation from ratio = 1 will suggest more or less growth at either end. In comparison with the histological data, the assumption of random EC regrowth shows close qualitative resemblance with the animal data and the growth along the stented length in that setting tends to remain moderately flat. The ratio plots of EC growth from both sides initially follow the *in vivo* data and random EC growth scenario trends near the reference point, but then it starts to deviate marginally (figure 6).

4. Discussion

In this study, histological (*in vivo*) neointimal growth patterns along the axial direction of the stent are compared with the computational simulations (*in silico*) to identify candidate

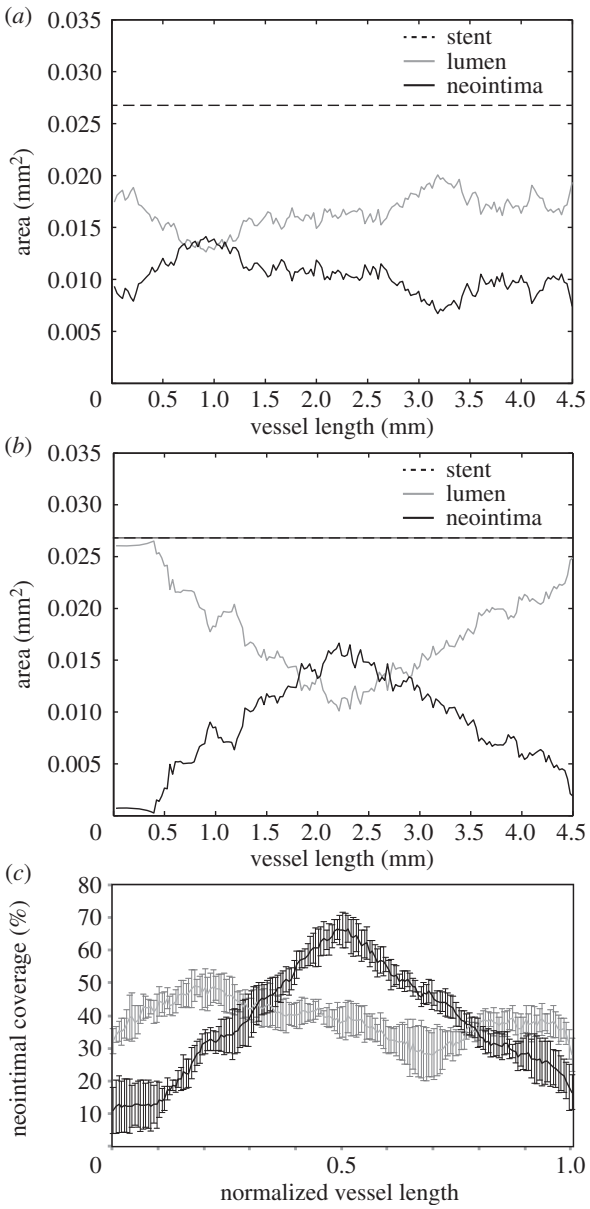

Figure 5. Area of the stent, lumen and neointima along the length of the stented region computed *in silico*. (*a*) Random seeding of ECs and (*b*) ECs regrowth from both sides inwards. (*c*) Percentage of neointimal growth based on the stent area after deployment for both re-endothelialization scenarios. Grey solid line shows the scenario of random EC seeding, whereas black solid line represents neointimal growth based on EC growth from both sides.

mechanisms for endothelial repair. Comparison of both *in vivo* and *in silico* results suggests that endothelial cell regeneration in coronary arteries after endovascular treatment is likely to be the outcome of EC growth from random EC seeding and/or patches of endothelium rather than cell growth and migration from either end of the stented region. Our comparison results (figure 6) strongly suggest that the neointimal ratio from the animal data does not support the hypothesis of the inward endothelium regrowth that results in reasonably higher centre-to-side ratios and dictates a higher neointima in the middle of the stented vessel. For ratio calculations, different reference points (ratio from centre to sides, or from sides to centre, etc.) can be used but the overall conclusion, showing a disagreement of the EC from both side scenario with the random EC and *in vivo* data, remains true.

It is also worthwhile to mention that some of the *in vivo* responses in figure 3*a* do not follow a straightline trend and,

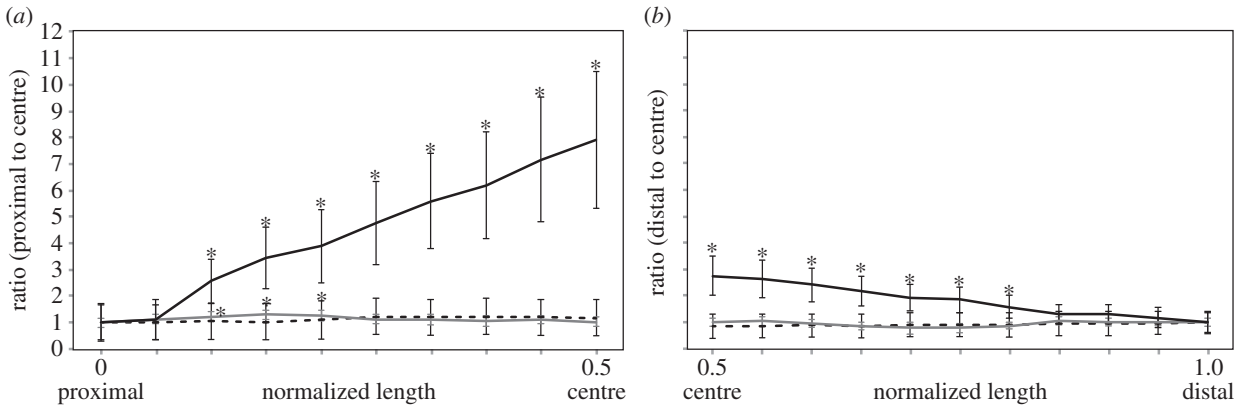

Figure 6. Comparison of the ratio trends between the animal data and two endothelium re-growth modelling scenarios based on the percentage of neointima inside the vessel. (*a*) Ratio from proximal to the centre and (*b*) ratio from distal to the centre. Black dotted line represents the *in vivo* data, solid grey line represents *in silico* random EC scenario and black solid line represents *in silico* EC from both sides scenario. All the data are presented as mean $\pm$ s.d. Black asterisk represents a statistical significant difference ($p < 0.05$) in the ratio calculations between the *in vivo* and the *in silico* EC from both sides scenario, whereas grey asterisk shows the data point which is significantly different ($p < 0.05$) between the *in vivo* and random EC scenario.

so linear regression may not be appropriate for all plots. The averaged value of the slope among all the arteries data was 0.035 ± 0.004 (neointimal area per normalized length). The averaged result from figure 3*a* is also shown in figure 3*b* where a slightly higher amount of neointimal growth on the distal side can be seen in comparison with the proximal side. Owing to the size of deviation in the averaged neointimal response, it is rather difficult to interpret the result though the overall growth response seems to stay fairly flat along the stent (figure 3*b*).

The literature specifically focusing on the endothelial growth process after vascular injury is rather sparse. To the best of our knowledge, there has been only one *in vivo* study undertaken by Itoh *et al.* [11] in the pial arteries of mice to specifically investigate the re-endothelialization process. In that study, a region of the endothelium was damaged via the photochemical reaction of rose Bengal to green laser light. Tie2-green fluorescent protein was used as a marker to identify live ECs. It was observed that the endothelium recovery process had already started within the first 24 h following endothelial injury and regeneration of the endothelium was observed from both edges (proximal and distal) of the denuded artery. Moreover, faster endothelial growth was observed from the proximal edge in comparison with the distal end, and the meeting point of endothelial layers from both sides was always distal to the centre of the injury, suggesting the differences in the re-endothelialization rate. The difference in the growth rate was due to flow direction where ECs were observed more elongated towards the flow direction and migrated and proliferated faster. Any apparent involvement of foreign progenitor cells in the EC repair process was not found, however, this could be related to the experimental set-up that was used in the study. Additionally, it is also worthwhile to mention that though the findings of Itoh *et al.* [11] are essential to understand the endothelium regrowth process, their model and set-up is not clinically relevant to the vascular stent-induced injury models and results may not be extrapolated directly to the coronary stenting experiments. Hence, we aimed to perform similar experiments in the porcine coronary-stented arteries in order to evaluate the endothelium regrowth process after the trauma induced by the balloon angioplasty and stent deployment.

We have used the findings of Itoh *et al.* [11] to describe one possible re-endothelialization scenario, assuming that ECs become functional in a similar fashion as they re-generate to form a lining on the vessel wall. Our modelling approach predicts that, under this scenario, neointimal growth in such an artery will result in a greater stenosis at the location where these edges meet each other. If both the findings shown by Itoh *et al.* [11] and the interactions between ECs, flow and SMCs assumed in the model are representative of *in vivo* conditions, then the histological data shown in figures 2, 3 and 6 are expected to show a peak in the growth process either at the centre of the stented vessel (based on our computational model assumption of identical growth rates at both proximal and distal sides) or somewhere distal to the centre (based on the observation of Itoh *et al.* [11]). However, the histological data do not seem to support the notion of EC inward growth alone as suggested by Itoh *et al.* [11]. The *in vivo* data presented here show stronger support for the scenario where endothelial regeneration occurs inside the stented region. In the biological experiments reported here, endothelial regeneration may include the involvement of both methods of EC regeneration (EC growth from both sides and from random patches/progenitors) acting together, as a result further controlled biological experiments are required to confirm the detail of this process.

Participation of EPCs towards endothelium regrowth is still an open question. Several studies have reported that endothelial regeneration is not mediated by the homing and differentiation of EPCs into mature ECs [9,11,32–34], however, they may facilitate the migration, elongation and proliferation of the resident ECs [11]. But, as we have shown, taking these observations into account and considering only that endothelium grows from both sides of the injury, we end up in a peak scenario that does not coincide with the neointimal growth patterns observed in the histology. According to Harnek *et al.*, a little endothelium in the denuded artery may survive the trauma caused by the balloon assisted stent deployment, so these patches may also contribute towards re-endothelialization. The *in vivo* study done by Itoh *et al.* [11] does not include the presence of healthy patches, instead, they induce a complete endothelial injury in the selected area of the vessel and the same approximation was taken in our computational model and this may explain the difference in results.

Another important observation from the evaluation of the histological neointimal growth reveals that a slightly higher growth was observed on the distal end when compared with the proximal side. This has been shown by linear regression analysis and a positive slope was observed in all the cases except one that showed a slightly negative slope. Although, a mismatch in stent–vessel size at the distal end resulting in deeper injury may account for exaggerated neointimal proliferation, it may also be due to the effect of the direction of flow on the endothelium regrowth process that mediates a faster growth from the proximal side of the injury and may also involve the flow direction-dependent growth from the leftover healthy patches. ECs directional migration and faster growth in the direction of flow have already been observed in several studies where EC become more elongated and proliferated faster in the flow direction; however, these studies do not focus on the neointimal growth [11,35,36].

Another obvious difference between the *in vivo* (figure 3) and the *in silico* (figure 5*c*) results is the variation in the magnitude of neointimal areas. The neointimal areas from the *in vivo* samples are in the range 20–80%, whereas those found *in silico* are roughly in the 30–50% range. In our opinion, there could be two reasons for these differences: (i) in the *in vivo* case, a stent is deployed into the artery and, depending upon the curvature and vessel dimensions, stent struts from the same stent impose different injury levels on the vascular wall. The neointimal thickness data shown in our previous paper [18] were obtained by analysing the injury on every strut in each histological section. During this analysis, we observed that different levels of injury are produced by stent struts within a single section. However, in the *in silico* model used in this study, we deployed struts at the same level into the tissue causing a similar injury over the whole domain. Such differences could lead to the differences in neointimal response. (ii) These differences may arise from simplification of the stent geometry from three to two-dimensional and may also be related to the stent properties (strut thickness, stent length, the orientation of the struts and stent porosity). All of these have been observed to affect the ISR growth, as described above, such factors can be assessed only quantitatively in a three-dimensional ISR model.

Our *in silico* model assumes static flow with $Re = 120$, which is the measured value at peak systole in pig coronary arteries [37]. Therefore, we do not capture the influence of the oscillatory shear index (OSI). It is known that high OSI results in disorganized endothelial morphologies [38] and sites of high OSI correlate with predominant sites of atherosclerosis. Note, however, that in our model the main concern is the repair of the endothelium and subsequent regulation of the SMCs via NO production, and for that process a high WSS value seems to be a main factor, and we believe that our static flow assumption does allow us to capture the main dynamics of the endothelial repair. However, we are currently setting up future *in silico* experiments to investigate the influence of real systolic flow conditions on the dynamics of ISR.

The basic two-dimensional model used in this paper has already been qualitatively validated in our previous papers [12,18] where the ISR growth trends in response to different levels of stent-induced injuries were qualitatively matched with the porcine *in vivo* data and results showed good agreement. Because the current computational study is limited to a two-dimensional ISR model, there is no direct comparison possible in terms of vessel dimensions (length and diameter) *in vivo* and *in silico* along with the differences in the number of struts present within the stented length; however, the aspect ratio (length versus diameter) of the vessel was kept similar in the *in silico* model (4.5 : 1) to measurements from the *in vivo* experiments (4.55 : 1). A better quantitative comparison is currently being undertaken in three dimensions, simulating ISR using *in vivo* stented vessel dimensions and full-length three-dimensional stents. The final goal of such studies to better understand the ISR patterns will be to include the vascular geometry that can be obtained directly from the imaging modalities and should be incorporated in the ISR three-dimensional model. This will allow us to model the blood flow in a more realistic domain taking into account the curvature of the vessel along with the accurate stent design. Modelling ISR in such realistic domains may better correlate with the neointimal patterns seen in the histology and allow us to do quantitative comparison which is far from trivial until now and should be taken as a next step forward in this research.

Finally, our study suggesting endothelial regeneration potentially from patches of surviving EC cells has potential clinical relevance. Stents vary in their design (open cell versus closed cell), strut dimensions (thickness and width) and metal-to-artery wall ratio. All these factors can influence the size of surviving EC patch and hence endothelial regrowth. It can partially explain the difference in endothelial coverage among first generation and newer stents, and may also help clinicians in making a more informed choice on selecting a particular stent for a patient and to develop better stents in future. Further studies with different stents are warranted.

5. Conclusion

Using a computational model of ISR and comparing with *in vivo* histology, we conclude that, within the context of the assumptions involved in the modelling process, endothelial growth from regions of the vessel proximal and distal to the stent is not sufficient to explain the morphology observed from histology. The results suggest that random EC seeding and/or patches of endothelium that survive balloon expansion and stent deployment play a role in endothelial recovery.

Acknowledgements. Conflict of interest: none declared.

Funding statement. This work was supported by the European Union Seventh Framework Programme (FP7/2007-2013) under grant agreement no. 238113 (project 'MeDDiCA'—'Medical Devices Design in Cardiovascular Applications'; http://www.meddica.eu/).

References

1. Serruys PW *et al*. 1991 Angiographic follow-up after placement of a self-expanding coronary-artery stent. *N. Engl. J. Med.* **324**, 13–17. (doi:10.1056/NEJM199101033240103)
2. Iqbal J, Gunn J, Serruys PW. 2013 Coronary stents: historical development, current status and future directions. *Br. Med. Bull.* **106**, 193–211. (doi:10.1093/bmb/ldt009)
3. Dangas GD, Claessen BE, Caixeta A, Sanidas EA, Mintz GS, Mehran R. 2010 In-stent restenosis in the drug-eluting stent era. *J. Am. College Cardiol.* **56**, 1897–1907. (doi:10.1016/j.jacc.2010.07.028)

4. Iqbal J, Sumaya W, Tatman V, Parviz Y, Morton A, Grech E, Campbell S, Storey RF, Gunn J. 2013 Incidence and predictors of stent thrombosis: a single-centre study of 5,833 consecutive patients undergoing coronary artery stenting. *Eurointervention* **9**, 62–69. (doi:10.4244/EIJV9I1A10)
5. Clopath P, Müller K, Stäubli W, Bürk R. 1979 *In vivo* and *in vitro* studies on endothelial regeneration. *Pathophysiol. Haemost. Thromb.* **8**, 149–157. (doi:10.1159/000214307)
6. Schwartz S, Haudenschild CC, Eddy E. 1978 Endothelial regneration. I. Quantitative analysis of initial stages of endothelial regeneration in rat aortic intima. *Lab Invest.* **38**, 568.
7. Asahara T, Masuda H, Takahashi T, Kalka C, Pastore C, Silver M, Kearne M, Magner M, Isner JM. 1999 Bone marrow origin of endothelial progenitor cells responsible for postnatal vasculogenesis in physiological and pathological neovascularization. *Circ. Res.* **85**, 221–228. (doi:10.1161/01.RES.85.3.221)
8. Asahara T, Murohara T, Sullivan A, Silver M, van der Zee R, Li T, Witzenbichler B, Schatteman G, Isner JM. 1997 Isolation of putative progenitor endothelial cells for angiogenesis. *Science* **275**, 964–966. (doi:10.1126/science.275.5302.964)
9. Hagensen MK, Vanhoutte PM, Bentzon JF. 2012 Arterial endothelial cells: still the craftsmen of regenerated endothelium. *Cardiovasc. Res.* **95**, 281–289. (doi:10.1093/cvr/cvs182)
10. Siddique A, Shantsila E, Lip GY, Varma C. 2010 Endothelial progenitor cells: what use for the cardiologist? *Vasc. Cell* **2**, 6.
11. Itoh Y, Toriumi H, Yamada S, Hoshino H, Suzuki N. 2010 Resident endothelial cells surrounding damaged arterial endothelium reendothelialize the lesion. *Arterioscler. Thromb. Vasc. Biol.* **30**, 1725–1732. (doi:10.1161/ATVBAHA.110.207365)
12. Tahir H, Bona-Casas C, Hoekstra AG. 2013 Modelling the effect of a functional endothelium on the development of in-stent restenosis. *PLoS ONE* **8**, e66138. (doi:10.1371/journal.pone.0066138)
13. Morton AC, Arnold ND, Crossman DC, Gunn J. 2004 Response of very small (2 mm) porcine coronary arteries to balloon angioplasty and stent implantation. *Heart* **90**, 324–327. (doi:10.1136/hrt.2003.015305)
14. Morton AC, Arnold ND, Gunn J, Varcoe R, Francis SE, Dower SK, Crossman D. 2005 Interleukin-1 receptor antagonist alters the response to vessel wall injury in a porcine coronary artery model. *Cardiovasc. Res.* **68**, 493–501. (doi:10.1016/j.cardiores.2005.06.026)
15. Malik N, Gunn J, Holt C, Shepherd L, Francis S, Newman C, Crossman DC, Cumberland DC. 1998 Intravascular stents: a new technique for tissue processing for histology, immunohistochemistry, and transmission electron microscopy. *Heart* **80**, 509–516.
16. Caiazzo A *et al*. 2011 A complex automata approach for in-stent restenosis: two-dimensional multiscale modelling and simulations. *J. Comput. Sci.* **2**, 9–17. (doi:10.1016/j.jocs.2010.09.002)
17. Evans DJW *et al*. 2008 The application of multiscale modelling to the process of development and prevention of stenosis in a stented coronary artery. *Phil. Trans. R. Soc. A* **366**, 3343–3360. (doi:10.1098/rsta.2008.0081)
18. Tahir H, Hoekstra AG, Lorenz E, Lawford PV, Hose DR, Gunn J, Evans DJW. 2011 Multi-scale simulations of the dynamics of in-stent restenosis: impact of stent deployment and design. *Interface Focus* **1**, 365–373. (doi:10.1098/rsfs.2010.0024)
19. Hegewald J, Krafczyk M, Tölke J, Hoekstra A, Chopard B. 2008 *An agent-based coupling platform for complex automata,* pp. 227–233. Berlin, Germany: Springer Computational Science-ICCS.
20. Hegewald J. 2010 The multiscale coupling library and environment (MUSCLE). See http://muscle.berlios.de/.
21. Borgdorff J, Falcone J-L, Lorenz E, Bona-Casas C, Chopard B, Hoekstra AG. 2013 Foundations of distributed multiscale computing: formalization, specification, and analysis. *J. Parallel Distrib. Comput.* **73**, 465–483. (doi:10.1016/j.jpdc.2012.12.011)
22. Borgdorff J, Mamonski M, Bosak B, Groen D, Belgacem MB, Kurowski K, Hoekstra AG. 2013 Multiscale computing with the multiscale modeling library and runtime environment. *Proc. Comput. Sci.* **18**, 1097–1105. (doi:10.1016/j.procs.2013.05.275)
23. Gunn J, Arnold N, Chan K, Shepherd L, Cumberland D, Crossman D. 2002 Coronary artery stretch versus deep injury in the development of in-stent neointima. *Heart* **88**, 401–405. (doi:10.1136/heart.88.4.401)
24. Johnson KL, Johnson KKL. 1987 *Contact mechanics*. Cambridge, UK: Cambridge University Press.
25. Popov VL. 2010 *Contact mechanics and friction: physical principles and applications*. Berlin, Germany: Springer.
26. Pathmanathan P, Cooper J, Fletcher A, Mirams G, Murray P, Osborne J, Pitt-Francis J, Walter A, Chapman SJ. 2009 A computational study of discrete mechanical tissue models. *Phys. Biol.* **6**, 036001. (doi:10.1088/1478-3975/6/3/036001)
27. Breton M, Berrou E, Brahimi-Horn M, Deudon E, Picard J. 1986 Synthesis of sulfated proteoglycans throughout the cell cycle in smooth muscle cells from pig aorta. *Exp. Cell Res.* **166**, 416–426. (doi:10.1016/0014-4827(86)90487-8)
28. Harnek J, Zoucas E, Carlemalm E, Cwikiel W. 1999 Differences in endothelial injury after balloon angioplasty, insertion of balloon-expanded stents or release of self-expanding stents: an electron microscopic experimental study. *Cardiovasc. Interv. Radiol.* **22**, 56–61. (doi:10.1007/s002709900329)
29. de Prado AP *et al*. 2011 Time course of reendothelialization of stents in a normal coronary swine model. *Vet. Pathol. Online* **48**, 1109–1117. (doi:10.1177/0300985811400446)
30. Guo X, Kassab G. 2009 Role of shear stress on nitrite and NOS protein content in different size conduit arteries of swine. *Acta Physiol.* **197**, 99–106. (doi:10.1111/j.1748-1716.2009.01999.x)
31. Nakazawa G *et al*. 2010 Anti-CD34 antibodies immobilized on the surface of sirolimus-eluting stents enhance stent endothelialization. *JACC Interv.* **3**, 68. (doi:10.1016/j.jcin.2009.09.015)
32. Tsuzuki M. 2009 Bone marrow-derived cells are not involved in reendothelialized endothelium as endothelial cells after simple endothelial denudation in mice. *Basic Res. Cardiol.* **104**, 601–611. (doi:10.1007/s00395-009-0021-7)
33. Hagensen MK, Shim J, Thim T, Falk E, Bentzon JF. 2010 Circulating endothelial progenitor cells do not contribute to plaque endothelium in murine atherosclerosis. *Circulation* **121**, 898–905. (doi:10.1161/CIRCULATIONAHA.109.885459)
34. Hagensen MK, Raarup MK, Mortensen MB, Thim T, Nyengaard JR, Falk E, Bentzon JF. 2012 Circulating endothelial progenitor cells do not contribute to regeneration of endothelium after murine arterial injury. *Cardiovasc. Res.* **93**, 223–231. (doi:10.1093/cvr/cvr278)
35. Ando J, Nomura H, Kamiya A. 1987 The effect of fluid shear stress on the migration and proliferation of cultured endothelial cells. *Microvasc. Res.* **33**, 62–70. (doi:10.1016/0026-2862(87)90007-0)
36. Simmers MB, Pryor AW, Blackman BR. 2007 Arterial shear stress regulates endothelial cell-directed migration, polarity, and morphology in confluent monolayers. *Am. J. Physiol. Heart Circ. Physiol.* **293**, H1937–H1946. (doi:10.1152/ajpheart.00534.2007)
37. Kassab GS, Berkley J, Fung Y-CB. 1997 Analysis of pig's coronary arterial blood flow with detailed anatomical data. *Ann. Biomed. Eng.* **25**, 204–217. (doi:10.1007/BF02738551)
38. Berk BC. 2008 Atheroprotective signaling mechanisms activated by steady laminar flow in endothelial cells. *Circulation* **117**, 1082–1089. (doi:10.1161/CIRCULATIONAHA.107.720730)